Electrostatics, proton sensor, and networks governing the gating transition in GLIC, a proton-gated pentameric ion channel

Haidai Hu[a,b], Kenichi Ataka[c], Anaïs Menny[d], Zaineb Fourati[a], Ludovic Sauguet[a], Pierre-Jean Corringer[d], Patrice Koehl[e], Joachim Heberle[c], and Marc Delarue[a,1]

[a]Unité Dynamique Structurale des Macromolécules, Institut Pasteur, UMR 3528, CNRS, 75015 Paris, France; [b]ED515, Paris Sorbonne Université, 75006 Paris, France; [c]Experimental Molecular Biophysics, Institute of Physics, Freie Universität Berlin, 14195 Berlin, Germany; [d]Unité Récepteurs-Canaux, Institut Pasteur, UMR 3571, CNRS, 75015 Paris, France; and [e]Department of Computer Science, Genome Center, University of California, Davis, CA 94520

Edited by Eric Gouaux, Oregon Health & Science University, Portland, OR, and approved November 19, 2018 (received for review August 3, 2018)

The pentameric ligand-gated ion channel (pLGIC) from *Gloeobacter violaceus* (GLIC) has provided insightful structure–function views on the permeation process and the allosteric regulation of the pLGICs family. However, GLIC is activated by pH instead of a neurotransmitter and a clear picture for the gating transition driven by protons is still lacking. We used an electrostatics-based (finite difference Poisson–Boltzmann/Debye–Hückel) method to predict the acidities of all aspartic and glutamic residues in GLIC, both in its active and closed-channel states. Those residues with a predicted pK_a close to the experimental pH_{50} were individually replaced by alanine and the resulting variant receptors were titrated by ATR/FTIR spectroscopy. E35, located in front of loop F far away from the orthosteric site, appears as the key proton sensor with a measured individual pK_a at 5.8. In the GLIC open conformation, E35 is connected through a water-mediated hydrogen-bond network first to the highly conserved electrostatic triad R192-D122-D32 and then to Y197-Y119-K248, both located at the extracellular domain–transmembrane domain interface. The second triad controls a cluster of hydrophobic side chains from the M2-M3 loop that is remodeled during the gating transition. We solved 12 crystal structures of GLIC mutants, 6 of them being trapped in an agonist-bound but nonconductive conformation. Combined with previous data, this reveals two branches of a continuous network originating from E35 that reach, independently, the middle transmembrane region of two adjacent subunits. We conclude that GLIC's gating proceeds by making use of loop F, already known as an allosteric site in other pLGICs, instead of the classic orthosteric site.

pentameric ligand-gated ion channel | pH activation | proton sensor | electrostatic networks | allosteric modulation

Pentameric ligand-gated ion channels (pLGICs), also known as Cys-loop receptors in animals, mediate rapid signal transduction in the central and peripheral nervous systems (1). Activation of these receptors is favored by the binding of agonists in the extracellular domain (ECD), which lowers the activation energy between closed and open states (2). This leads to a global allosteric conformational change and promotes the opening of the transmembrane domain (TMD) ion channel pore. Dysfunction of pLGICs can cause severe nervous-system diseases and conditions, such as Alzheimer's disease, Parkinson's disease, epilepsy, and alcohol dependence. They are the targets of several important therapeutic compounds, such as general anesthetics, barbiturates, and benzodiazepines, whose structures of complexes with a pLGIC are reviewed in ref. 3.

Available structural information on this family was derived from a number of prokaryotic and eukaryotic channels (4–12). Because the disulfide bridge of the Cys-loop is not conserved in prokaryotes and only one proline is absolutely conserved in this loop in pLGICs, it was suggested recently that they be called Proloop receptors (13). Despite substantial diversity of sequences, structural information shows high conservation of tertiary and quaternary architectures between eukaryotic receptors and their bacterial homologs. Besides the covalent link between the ECD and TMD through the pre-M1 region, the ECD–TMD interface comprises four highly conserved loop regions: the β1-β2 loop, the loop F, the Cys-loop, and the M2-M3 loop (Fig. 1*A*, *Inset*). Of all pLGICs, the prokaryotic ELIC from *Erwinia chrysanthemi* and GLIC from *Gloeobacter violaceus* stand out as the subjects of many structure–function relationship studies. Notably, GLIC has been captured in four different states. Following the first apparently open/active state of GLIC crystallized at pH 4.0 (12, 14), several proton-bound but nonconducting forms have been solved, which have been designated as "locally closed" states (LC) (15–17). Among those LC forms, which all display an unfolding of the C terminus of the M2 helix and a change of its orientation that closes the pore but have different conformations of M2-M3 loop, one of them (LC2) has been recently suggested to be a preactive state, an intermediate state along the transition pathway from the resting state to the active state (18). The closed/resting state of GLIC was solved at neutral pH (19). Finally, the structure of a putative desensitized state of GLIC has also been reported (20). In addition, GLIC has been extensively used to characterize the

Significance

Several classes of membrane ion channels are sensitive to the intracellular or extracellular proton concentration. However, the detailed mechanism of channel gating induced by protonation proves in general difficult to address. Here we use a combined computational and experimental approach to identify the proton sensor in the pentameric proton-gated ion channel GLIC. Further electrophysiology and crystallography data help delineate the mechanism of the gating transition initiated by protonating this sensor, revealing that those positions that trap the receptor in a nonfunctional closed-pore conformation build up a continuous network. Our results provide an approach to search for and identify proton sensors as well as networks of residues important for the gating transition in the pentameric ligand-gated channels family.

Author contributions: M.D. designed research; H.H., K.A., A.M., J.H., and M.D. performed research; H.H., K.A., A.M., Z.F., L.S., P.-J.C., P.K., J.H., and M.D. analyzed data; and H.H., K.A., A.M., and M.D. wrote the paper.

The authors declare no conflict of interest.

This article is a PNAS Direct Submission.

Data deposition: The atomic coordinates and structure factors have been deposited in the Protein Data Bank, www.pdb.org (PDB ID codes 6HZW, 6HY5, 6HYR, 6HY9, 6HYA, 6HYX, 6HYV, 6HYW, 6HYZ, 6HZ0, 6HZ1, 6HZ3, 6I08) and are listed in *SI Appendix*, Table S3.

[1]To whom correspondence should be addressed. Email: marc.delarue@pasteur.fr.

This article contains supporting information online at www.pnas.org/lookup/suppl/doi:10.1073/pnas.1813378116/-/DCSupplemental.

Published online December 12, 2018.

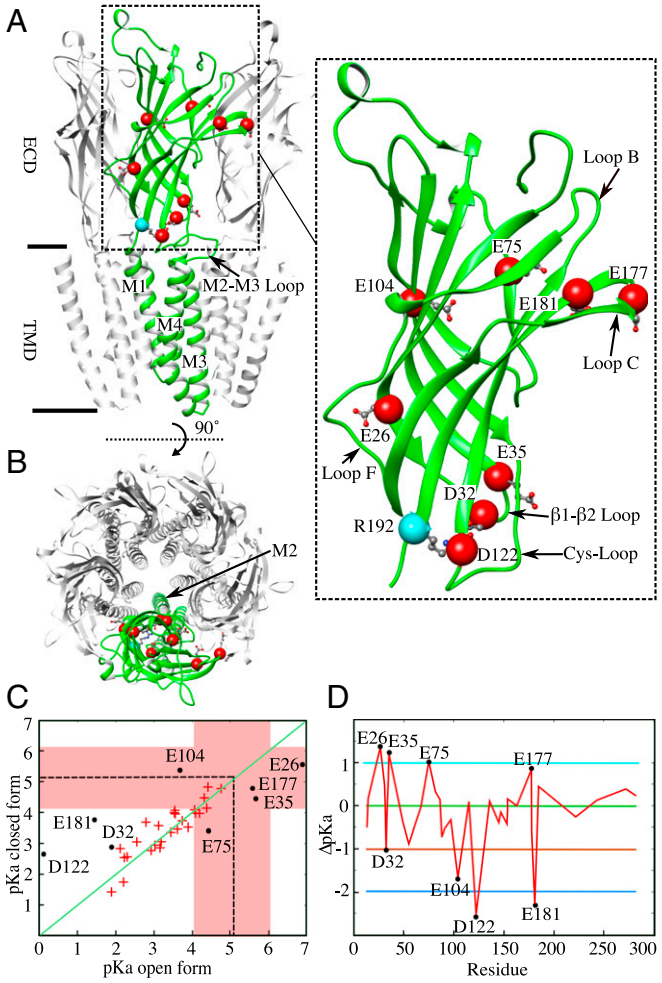

Fig. 1. Predictions of proton-sensing residues among all Glu and Asp in GLIC derived from electrostatic FD/DH calculations. (*A*) Cartoon representation of the open form of GLIC crystallized at pH 4. The front subunit is highlighted and shown in green. Asp and Glu residues predicted to have ΔpK_a larger than one unit between the open and closed states are shown as sticks and their Cα atoms are shown as red van der Waals spheres (*Inset*). Cα atom of R192 is shown as a cyan sphere. The black bars represent the plasma membrane level. (*B*) Top view of GLIC with color and representation of atoms identical to *A*. (*C*) Scatter plots for the predicted pK_a values of all Asp (19 for each subunit) and Glu (16 for each subunit) for the open and closed forms of the receptor (red crosses). Residues deviating from the diagonal by more than one pH unit (black dots) are labeled. Residues lying on the diagonal (green line) have predicted pK_a values that are equal in the two forms. The pink region contains residues for which the protonation state is predicted to change at $pH_{50} \pm 1$ ($pH_{50} = 5.10 \pm 0.20$). (*D*) ΔpK_a values, from the open to closed form, of Asp and Glu are plotted as a function of the residue number (red line).

binding properties of important pharmacological reagents, such as propofol (21), bromoform (22, 23), ethanol (22, 24), and barbiturates (25), while ELIC has also been used for the structural characterization of the binding of general anesthetics and benzodiazepine molecules (26–28). A number of biophysical methods, such as electron paramagnetic resonance, have also been applied to characterize GLIC conformations in solution. These methods, due to their inherent time scale, are likely to probe the desensitized state, whose structure is still highly debated, leading to some apparent disagreement in the interpretation of the experiments (29–32).

GLIC's channel is gated by protons with $pH_{50} = 5.1 \pm 0.2$, at which half of the maximal current amplitude is reached. This contrasts with most human pLGICs, which are activated by neurotransmitter binding to a cavity in an intersubunit interface in the ECD, mainly involving loops B and C (Fig. 1*A*, *Inset*). Various invertebrate pLGICs have been demonstrated to be directly responsive to pH (33–35). Proton-gating has also been observed in ion channels that are not members of the pLGIC family, such as acid-sensing ion channels and some inward-rectifying potassium channels (Kir) (36, 37). The mechanism of proton gating is in general very difficult to study, as there are many candidates for the role of proton-sensing residues. In addition, protons are usually not directly seen by crystallography, precluding the possibility to ascertain which residue is protonated and which is not, even if the structure is known at high resolution.

In this study, we performed a systematic and computer-aided survey of residues that can be qualified as proton sensors contributing to channel gating in GLIC, namely residues that change their protonation state during the conformational transition. Taking advantage of the knowledge of the structures of open/active and closed/resting forms of GLIC, we use the finite difference Poisson–Boltzmann/Debye–Hückel (FD/DH) to predict individual pK_a values and to guide the search for the position of pH-sensing residues. FD/DH has been shown to be superior to classic finite difference Poisson–Boltzmann (FD-PB) (38) for filtering candidate residues responsible for pH-induced channel gating. We then experimentally determined the individual pK_a values of those residues that exhibit a strong change in the calculated pK_a values between the two known states, by employing attenuated total reflectance (ATR) Fourier transform infrared spectroscopy (FTIR). The assignment of the carboxylic side-chain frequencies was performed by replacement of individual carboxylate residues by alanine and calculating the difference between the spectra of the wild-type and mutated receptors. We infer from these results that E35 accounts for proton sensing, in accordance with recent electrophysiology results (39).

We then explored the environment of residue E35, located at the ECD–TMD interface with loop F of the adjacent subunit, by mutagenesis, chemical labeling, electrophysiology, and structural analysis and found an interfacial hydrogen network mediated by water molecules, which controls channel gating, in association with an additional layer made of an intrasubunit cluster of hydrophobic side chains. Both networks are crucial for maintaining the channel open. These networks can be mapped further down to the middle pore region in two adjacent subunits by projecting on the structure of the active state of GLIC all known positions whose mutation results into an LC structure, namely a structure trapped before the transition to the active form.

Results

Poisson–Boltzmann Electrostatics and the FD/DH Method Predict Potential pH-Sensing Residues in GLIC. Activation of GLIC is triggered by lowering the pH from neutral to acidic values with a $pH_{50} = 5.1 \pm 0.2$. Our goal is to identify those residues whose protonation will most profoundly affect the conformational transition between the closed and the open forms of the channel. These are likely to be either Asp, or Glu or His residues. There are 34 carboxylate residues in each subunit, along with 3 His residues. Here we focus on Asp and Glu as it has been shown elsewhere that His residues play no role in the gating transition (39). It is expected that the pK_a values of carboxylate residues that are essential to proton activation should be significantly shifted from their model pK_a (Asp = 3.8–4.0; Glu = 4.2–4.4). However, this is a necessary but not sufficient condition to predict/identify the proton-sensing residues. Indeed, following Sazanavets and Warwicker (38), one can divide residues whose pK_a values are shifted from their model pK_a in two classes: pH-sensors and pH-coupled. Only the pH-sensors are expected to change ionization during the conformational change between the two forms, namely around $pH_{50} \pm 1$, whereas proton-coupled residues are not (38).

PB electrostatic calculations can predict individual pK_a values of a protein with a known structure. FD/DH calculation is a refined PB method that has been shown to be significantly better at predicting pH-sensing residues compared with normal FD-PB methods (38). For charged and exposed residues, the method takes into account both their intrinsic flexibility by sampling all possible rotamers as well as the screening effect due to the surrounding salt by using the DH theory (38). GLIC X-ray structures have been solved in both its open/active form (pH 4.0, PDB ID codes 3EAM and 4HFI) and in its closed/resting form (pH 7.0, PDB ID code 4PQN) so that we can calculate pK_a values in both forms.

The FD/DH analysis of all GLIC carboxylate protonatable residues shows that most have the same predicted pK_a values in both states (Fig. 1*C* and *SI Appendix*, *Supplementary Notes*), suggesting that they are not involved in pH sensing. Interestingly, five Glutamate residues (E26, E35, E75, E104, and E177) are predicted to change protonation state within one log of the functional pH_{50} and have a predicted pK_a value significantly different in the two states (pink zone in Fig. 1*C*). E177 is located near the known agonist-binding site (loop C), while E26, E35, and E75 are at the interface between two subunits. E104 is located close to a known positive allosteric modulator (PAM) binding site (Fig. 1*A*, *Inset*).

In comparison, the pK_a values of D32, D122, and E181 differ substantially between the open and the closed forms ($\Delta pK_a \geq 1$), but in a pH range distant from GLIC's pH_{50} (Fig. 1 *C* and *D*), and are therefore more likely to be pH-coupled residues rather than pH-sensing (38). D32 and D122 are involved in strong electrostatic interactions with R192, which are highly conserved in almost all pLGIC, even in receptors that are not activated/modulated by pH changes (13). Mutations at these positions often impair the expression of the receptors at the cell membrane or lead to total loss-of-function phenotypes (*SI Appendix*, Table S1). Therefore, they are not expected to play a role in proton sensing per se but rather to be essential for maintaining the structural integrity of the receptor. E181 is located in loop C, which experiences a considerable conformational change between the two states and would be a good candidate for proton sensing (*SI Appendix*, Fig. S2*B*). However, its predicted pK_a is not in the range of $pH_{50} \pm 1$. Furthermore, mutations of each protonatable residue in loop C show no or small effects on proton activation in the range of pH 7.0–4.0 (40, 41). Indeed, deleting the entire loop C or replacing it by 10 glycines does not affect pH activation of GLIC (17).

The output of FD/DH calculations contains a list of putative salt bridges and strong hydrogen bonds in the structure, along with their calculated energy. The strongest ion pairs (with an interaction energy around 9 kT in the open form, but 6 kT in the closed form) involve the triad R192, D122, and D32, a strongly conserved feature of all pLGICs (13). Interestingly, the less-known triad made of Y197-Y119 within the same subunit and K248 of the next subunit is at the same energy level (8.5–9.5 kT). These two triads, hereafter referred to as primary and secondary triads, respectively, are linked together by an interaction between Y197 and R192 of 4.8–5.2 kT in the open form (but not in the LC forms). The interactions between K248 and Y119 or Y197 are weakened in the closed form (*SI Appendix*, *Supplementary Notes*).

To further characterize the potential candidates for pH-sensing (E26, E35, E75, E104, E177), titrations using FTIR spectroscopy in combination with site-directed mutagenesis were performed to experimentally derive their individual pK_a values, because these quantities cannot be derived easily from electrophysiology experiments. Other residues (D86, D88, E67, D97, E181, and E243) served as experimental controls (*SI Appendix*, Fig. S3).

Experimental Determination of the Individual pK_a Values of Potential pH-Sensing Residues by ATR/FTIR Spectroscopy. FTIR spectroscopy of the pH-induced conformational transition of GLIC has been conducted using the ATR sampling technique (*SI Appendix*, Fig. S1*A*). Wild-type GLIC and its mutants have been reconstituted in a mixture of palmitoyloleoyl phosphatidylethanolamine (POPE) and palmitoyloleoyl phosphatidylglycerol (POPG). Protein–lipid films were dried atop the internal reflection element and immersed in buffered aqueous solution. Difference spectra were calculated between sample spectra measured at various low pH values down to pH ∼2.0 and a reference spectrum measured at pH = 7.0. Peak positions of the bands in the FTIR spectra of the wild-type and the E35A mutant (Fig. 2 *A* and *B*) are almost identical, with differences smaller than 2 cm^{-1}. All observed bands could be assigned either to the protein (1,718–1,722, 1,655, 1,630, 1,573, 1,540, 1,520, 1,400 cm^{-1}), to the lipids (1,738, 1,466, 1,456 cm^{-1}), or to the buffer (1,364, 1,321, 1,218 cm^{-1}), as described in *SI Appendix*, *Supplementary Materials and Methods*. Among the protein bands, those at ∼1,720 cm^{-1} [ν(C = O)], ∼1,573 cm^{-1} [$\nu_{as}(COO^-)$], and 1,400 cm^{-1} [$\nu_s(COO^-)$] are assigned to the carboxylic acid/carboxylate group of Asp or Glu residues. An increase in the intensity of the ν(C = O) band due to the carboxylic acid (1,720 cm^{-1}) is observed at lower pH because of its protonation, along with the decrease of the intensity of $\nu_{as}(COO^-)$ and $\nu_s(COO^-)$ bands. Because the intensities of these bands indicate the extent of the protonation state of Asp and Glu residues in the protein, a plot of the intensity of these peaks as a function of pH provides a titration curve for the carboxyl groups. We note that a definite determination of peak positions and absolute intensities of ν(C = O) and $\nu_{as}(COO^-)$ are difficult to obtain because these bands closely overlap with a lipid ester band at 1,738 cm^{-1} and amide II band at 1,540 cm^{-1}, respectively. Therefore, we used the $\nu_s(COO^-)$ band at 1,400 cm^{-1} as a marker for the intensity analysis of carboxylic group, as it is sufficiently isolated from other bands (Fig. 2 *A* and *B* and *SI Appendix*, Fig. S1 *B–E*).

See Fig. 2*C* for the normalized peak heights at 1,400 cm^{-1} for the wild-type (black cross in Fig. 2*C*) and E35A mutant of GLIC (red dots in Fig. 2*C*). The intensities are normalized to be 0 at pH = 7.0 and −1 at pH 2.0 for the wild-type GLIC receptor. These plots provide a titration curve of all Glu and Asp residues in GLIC. Because each GLIC subunit contains 16 Glu and 18 Asp residues, the overall titration curve displays a broad sigmoidal shape in a wide range of pH values due to the overlap of the individual titration curves from each residue. Notably, the pH titration curve from the E35A mutant shows significant deviations from that of the wild-type receptor (Fig. 2 *C* and *D*). Note that individual features of these titration curves are highly reproducible in a set of three independent experiments (*SI Appendix*, Fig. S4).

The differences in the pH titration curves become clear when the trace from the wild-type is subtracted from each of the mutant's trace. In a first approximation, one can show that the difference between the titration curves of the mutant and the wild-type represents the titration of the individual group that has been replaced by an alanine. The deviation of the traces is in the range of 2–7% of the total intensity (Fig. 2*D*). Deviations in curves from the wild-type receptor between two different experiments do not exceed the range of ±1%. Therefore, we only consider mutants whose titration curves exhibit deviations >2%, as seen in the E35A and E181A variants. The other variants, E26A, E75A, E177A, and E104A, are below this criterion; thus, we do not attempt to derive a pK_a value for these groups (Fig. 2*D*). Experimental pK_a values of E35 and E181 residues were determined to be 5.8 and 5.5, respectively, through fits to the Henderson–Hasselbalch equation (continuous lines in Fig. 2*D*).

We note that the trace of E35A (Fig. 2*D*) exhibits a sigmoidal shape, as expected for a canonical pH titration involving one proton. The abrupt decrease observed from pH 4.2–3.0 is not caused by an artifact caused by the instability of the lipid bilayer, as shown by the difference spectrum of the E243G mutant, which has a normal titration curve that is flat from pH 2.5–4 (*SI Appendix*, *Supplementary Notes*). Rather, the decrease of the signal

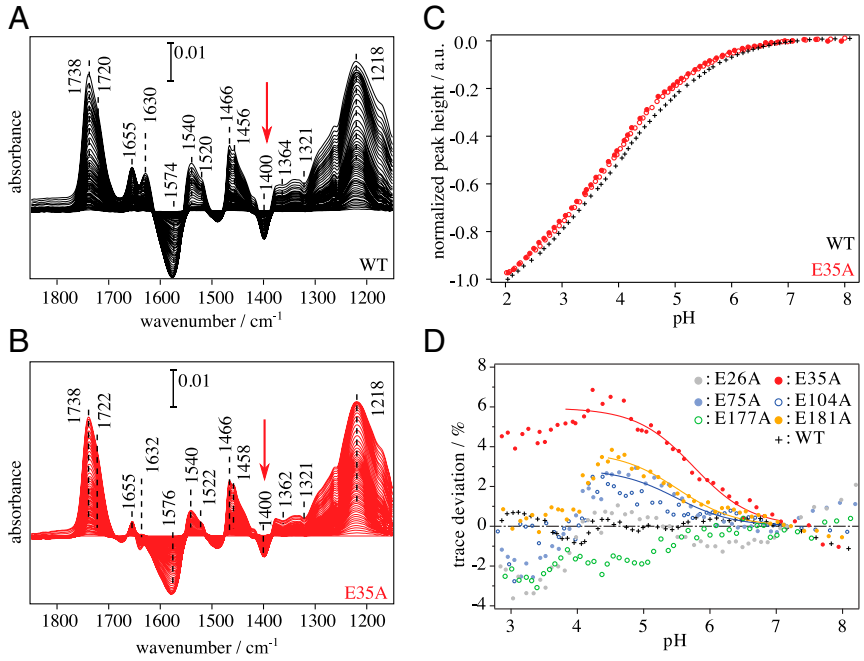

Fig. 2. pH-induced FTIR difference spectra of GLIC reconstituted in POPE/POPG lipids of (*A*) wild-type GLIC and (*B*) the E35A mutant. Reference spectra were taken at pH = 7.0 and FTIR differences were recorded while the solution pH was continuously lowered. Negative peaks represent the structural components that were reduced after lowering the pH, while positive peaks represent the structural components that were gained by lowering the pH. (*C*) pH titration curves derived from the normalized intensities of the band at 1,400 cm^{-1} (symmetric carboxylate vibration) of the wild-type (+) and of the E35A mutant (red). Open and filled symbols represent data from different experiments performed under identical conditions. (*D*) Deviations of the mutants' pH titration from the wild-type. The cross marker in black (+) represents trace deviation of wild-type between two different experiments, which sets the extent of the reproducibility error. The solid curves represent results of fitting the data points by the Henderson–Hasselbalch equation for E35A, E75A, E181A.

at pH < 4.2 can be explained by the change in pK_a of one of the protonatable groups accessible to the solvent, induced by the mutation itself (*SI Appendix*, *Supplementary Notes*). This adds a negative "bell-shaped curve" centered at around pH 3.8–4.2, on top of the regular pH-induced titration curve. Theory predicts that the pK_a^{eff} of E181 should be equal to $pK_a^{(c)} - \log K_D$, which directly leads to an estimate of $K_D = 20$, where K_D is the equilibrium constant between the open and closed forms at pH 7 (*SI Appendix*, *Supplementary Notes* and Eq. S14). For this particular pLGIC, FTIR allowed to experimentally determine K_D, which is of course a crucial quantity in the classical allosteric model.

Probing Residues Around E35 by Site-Directed Mutagenesis. Among the potential proton-sensing residues (pink zone in Fig. 1*C*), E35 stands out as the only one whose individual pK_a could be precisely measured with a well-defined transition curve by FTIR, and its pK_a value is indeed close to the pH_{50} determined by electrophysiology. Because E35 is not located at or close to the expected agonist-binding site of the pLGIC family, delineated by loop C and loop B, we performed a systematic study of its immediate environment by mutagenesis.

Exploring the role of loop F by mutation and chemical labeling. Examination of the structure of GLIC indicates that E35 establishes a polar interaction with T158 from loop F (Fig. 3*A*, *Inset*). To determine whether this interaction belongs to a network of interactions important for the global allosteric transition involved in gating, we probed this residue as well as those immediately adjacent in loop F (G159, W160) by site-directed mutagenesis. Each position was mutated to a cysteine to perform further analysis through chemical labeling, and the impact of these mutations on the function of the corresponding residue was measured by electrophysiology. The Cys-less mutant of GLIC (C27S) has the same properties as the wild-type GLIC and is unaffected by treatment with *S*-methylmethanethiosulfonate (MMTS), a reagent that blocks the side chain of cysteine and converts it into $–S-S-CH_3$ group, or with DTT, which reduces S-S bonds. Cysteine replacement of T158 does not affect the function of the receptor. However, when the T158C mutant is labeled with MMTS, the current is decreased by 50%. This phenotype can be reversed by reducing and removing the MMTS labeling (Fig. 3*B*). G159C mutation totally abolishes the pH-induced currents and generates a nonfunctional receptor; this is also the case of the W160C mutant (*SI Appendix*, Table S2). Expression tests in oocytes show that W160C is not expressed and G159C has a low expression level, but still detectable (*SI Appendix*, Fig. S11), indicating that the two residues located in loop F are not only functionally important but also structurally crucial for the receptor. Notably, the side chain of W160 is stacked above the strictly conserved residue R192 (see, for example, Fig. 5*A*). We noted earlier that the TGW sequence in GLIC's loop F is special, where it is usually [G]EW in cationic pLGICs (42) (see, for example, Fig. 6*B*).

A water-mediated electrostatic network at the ECD–TMD interface stabilizes the open-form structure. An open-form crystal structure of GLIC was determined at 2.22-Å resolution and has significantly better refinement statistics than the previously known 2.4-Å structure (*SI Appendix*, Table S3), which allows a more detailed study of the bound water molecules. A close analysis of this high-resolution model uncovers the existence of an elaborate hydrogen-bond network at the ECD–TMD interface. The side chain of Q193 interacts with the backbone amide nitrogen atom of G159 from loop F, as well as with the carbonyl oxygen atom of K248 from the M2-M3 loop of the adjacent subunit through hydrogen bonds mediated by water molecules. This hydrogen-bond network at the ECD–TMD interface extends to residue T158 of loop F, which is in turn interacting with E35 (Fig. 3*A*, *Inset*).

Probing the interfacial hydrophilic crevice centered on Q193. Q193 has been replaced by a hydrophobic residue, either methionine or leucine. Electrophysiology experiments show that both mutants

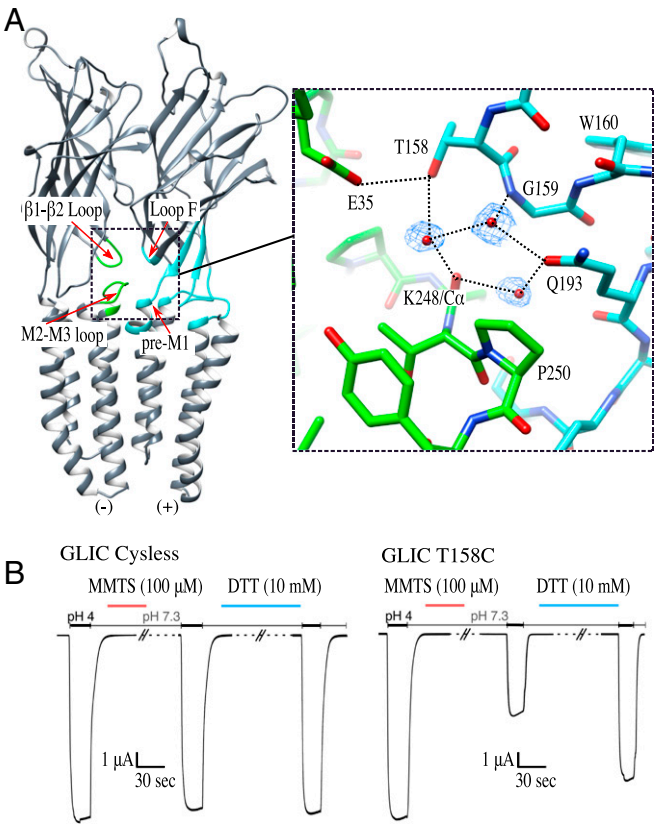

Fig. 3. Probing the immediate environment of E35. (*A*) Cartoon representation of the open form at 2.22-Å resolution for GLIC at pH 4. Only two subunits, viewed from the outside of the pentamer, are shown. The ECD and TMD interface loop regions are highlighted in green and blue. The *Inset* shows structurally ordered water molecules at the ECD–TMD interface crevice. Water molecules are depicted as red spheres with blue mesh representation of 2m*Fo*-D*Fc* electron density map contoured at a level of 1 σ and overlaid. Surrounding residues are represented as sticks and labeled. Black dashed lines represent the hydrogen-bonds network at the domain interface made of water molecules, loop F, Q193, and the M2-M3 loop. (*B*) Effect of MMTS binding on the function of GLIC Cys-less and mutant T158C. The same recording protocol was used for all constructs (*Materials and Methods*).

exhibit a loss-of-function phenotype with $pH_{50} = 4.53 \pm 0.02$ and $pH_{50} = 4.48 \pm 0.05$ compared with that of wild-type $pH_{50} = 5.10 \pm 0.20$ (Fig. 4*A* and *SI Appendix*, Table S2). We solved the crystal structures of Q193M and Q193L at pH 4 with 2.95-Å and 3.39-Å resolution. Unexpectedly, both mutants adopt the conformation previously described as LC1 in the LC (15) or "fully liganded closed-channel" forms (16). When superimposed to GLIC H235F, the very first LC1 form of GLIC (PDB ID code 3TLC) (15), the Q193M and Q193L mutants show an RMSD of 0.61 and 0.59 Å, respectively. All five M2 α-helices are kinked at the level of the I9′ position. The upper portion of M2 helices tilts and rotates clockwise around the fivefold symmetry axis along the ion-channel pore, and consequently narrows the ion-permeation pathway, generating a nonconductive ion channel (Fig. 4 *C*, *E*, and *F*). Compared with the wild-type open-form structure, the side chains of M193/L193 rotate by 90° and do not protrude into the interfacial crevice any more (Fig. 4*D*). Thus, breaking the hydrogen-bond network by replacing Q193 with hydrophobic residues hinders gating and destabilizes the open form.

We further probed the ECD–TMD interfacial hydrogen-bond network by replacing Q193 with a cysteine to introduce a shorter and less polar side chain. The phenotype of Q193C was almost identical to that of the wild-type (*SI Appendix*, Table S2). Consistently, the 2.58-Å resolution structure of Q193C adopts the open conformation at pH 4 (*SI Appendix*, Fig. S7*A*). The structure shows a water molecule in the interfacial crevice region that connects the thiol group of C193 to the nitrogen atom of G159 and to the nitrogen atom of P250 of the neighboring subunit (*SI Appendix*, Fig. S7*B*, *Inset*). The resulting hydrogen-bond network was probed by additional experiments to confirm its putative role in maintaining the channel open. Labeling Q193C with MMTS leads to a 75% current decrease, which is reversed by DTT reduction. Thus, breaking the new interfacial hydrogen-bond network destabilizes the open form of the channel. Next, the cocrystallized structure of Q193C with MMTS

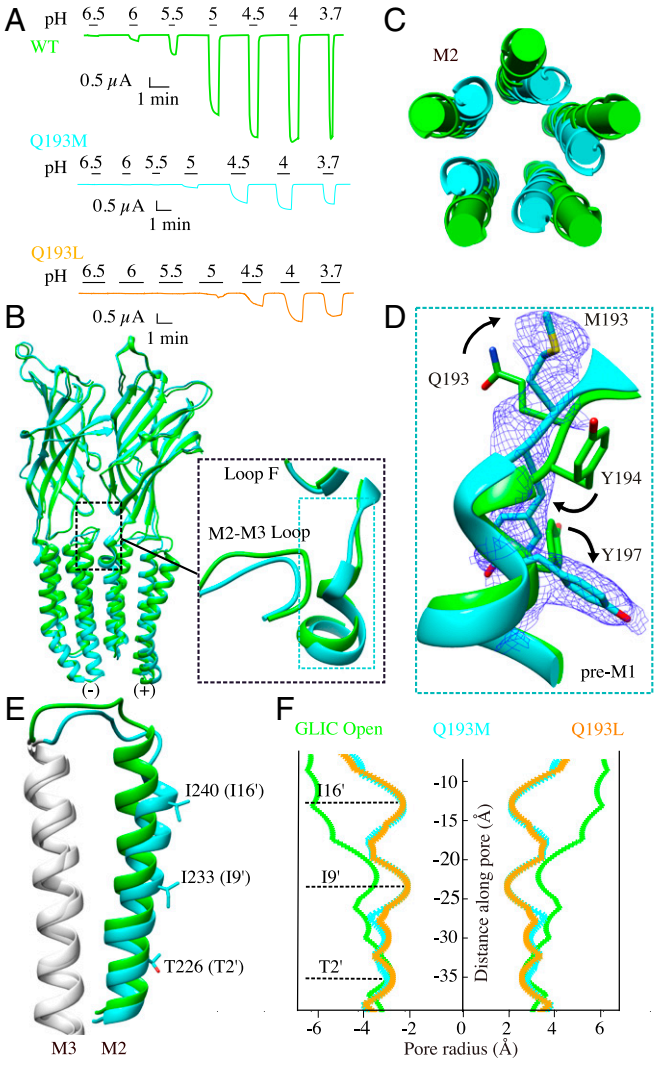

Fig. 4. Characterization of GLIC Q193M and Q193L mutations. (*A*) Proton-elicited currents from GLIC wild-type (green), Q193M (cyan), and Q193L (orange). (*B*) Structural superimposition of the GLIC Q193M (cyan) with the open form of wild-type GLIC (green). Only two subunits are shown viewed from the outside of the pentamer. Both structures are aligned using the whole pentamer. *Inset* shows an enlarged view of the pre-M1 region and of the M2-M3 loop reorganization. (*C*) Top view of the conformational change of M2 helices. (*D*) Conformational rearrangement of the pre-M1 region. The electron density of the 2m*Fo*-D*Fc* map around Q193M (blue) is contoured at the level of 1 σ. (*E*) Side view of the conformational change of the M2 helix, M2-M3 loop, and M3 helix from one subunit. (*F*) Pore-radius profile for GLIC WT open (green), Q193M (cyan), Q193L (orange). The constriction sites in the LC conformation from M2 helix are labeled and are shown as sticks in *E*.

shows a conformation similar to that Q193M (*SI Appendix*, Fig. S7 *C* and *D*) and the 2m*Fo*–D*Fc* map shows density for the MMTS covalently linked molecule (*SI Appendix*, Fig. S5 *E* and *F*). In addition, we tried to enhance the interaction of Q193C with the M2-M3 loop by introducing a second cysteine residue (P250C), in a position such that it could form a disulfide bridge with Q193C. As predicted, this double mutation shows a strong gain-of-function phenotype. In oocytes expressing GLIC Q193C-P250C receptors, the recording shows an apparent leak of current at pH 7 that can be blocked by picrotoxin, an open channel blocker (*SI Appendix*, Fig. S8*C*), and abolished by treatment with DTT. All of this evidence points to the key role of the residue Q193 located at pre-M1 region in coupling proton binding to channel opening.

Preceding Q193, residue R192 interacts with two negatively charged residues: D122 and D32. This triplet forms a bifurcated salt bridge that is conserved among pLGIC receptors and has been shown to be functionally important for channel activation (17, 43). Furthermore, the 2.22-Å structure clearly shows that the water molecule network linking E35 to Q193 can be further extended to Y197 and R192 (*SI Appendix*, Fig. S5). While the apolar atoms of the side chain of the strictly conserved P120 (Cys-loop) interact with those of Y119 and Y197 through hydrophobic interactions, the hydroxyl group of Y197 interacts with the side chain of R192 (*SI Appendix*, Fig. S5, *Inset*). Therefore, residues Y197-K248-Y119 form a secondary electrostatic triad that interacts with the primary one in the open form.

Probing the Tyrosine Residues from the Secondary Electrostatic Triad at the ECD–TMD Interface. The FD/DH method predicts that the two tyrosine from the secondary electrostatic triad have a highly ΔpK_a value (*SI Appendix*, Fig. S9). At the structural level, Y197 stands out as undergoing a switch of its side chain from an "inward" position to an "outward" position when switching from the LC1 form to the open form. During this rearrangement of the pre-M1 region, Y194, which points toward the lipid bilayer in the open form, also flips its orientation by almost 180° and becomes buried inside the intersubunit cavity (Fig. 4*D*). This breaks the interaction of Y197 with R192. To test whether both the hydroxyl and aromatic groups are required for proton-elicited channel currents, we mutated Y197 to phenylalanine and alanine separately.

The pH 4 crystal structure of the Y197F mutant is identical to that of Q193M/Q193L, with the side chains of Y194 and Y197F adopting the same conformations as in the model of Q193M/Q193L (Fig. 5 *C*–*E*). However, on the functional level, Y197F does not show any decrease in proton sensitivity, with a pH_{50} identical to the wild-type GLIC (Fig. 5*B* and *SI Appendix*, Table S2). This suggests that even though the activation barrier between the LC form and the open form is increased, it can still be crossed to lead to the open conformation of the channel in solution, contrary to what is seen in Q193M/Q193L. Since the aromatic ring of Y197 interacts with P120 (Cys-loop), Y119 (Cys-loop), and L246 (M2-M3 loop) through hydrophobic or stacking interactions, we replaced Y197 by an alanine (Y197A) to disrupt the interaction between Y197 and R192, and to reduce the hydrophobic stacking between both the Cys-loop and the M2-M3 loop. The Y197A mutation completely abolishes the function of the channel (Fig. 5*B* and *SI Appendix*, Table S2). We could only get a 7-Å dataset from crystals of Y197A, but we could nevertheless assess that Y197A mutation traps the receptor in the LC form (*SI Appendix*, Fig. S10). Hence, our data indicate that the aromatic residue Y197 plays a crucial role in the coupling of proton binding to channel gating.

Y119 is predicted to also have a large ΔpK_a value (*SI Appendix*, Fig. S9*B*). The crystal structure of Y119F displays an open conformation, which is in line with functional recordings that show a wild-type phenotype. Furthermore, the 2.8-Å crystal structure of the Y119A mutant that generates a nonfunctional receptor (17) adopts an open conformation (Fig. 5 *F* and *G*), but with additional strong and continuous electron density in the Fourier m*Fo*–D*Fc* difference map near the mutation site (average peak height at 7.5 σ), indicative of the presence of a bound

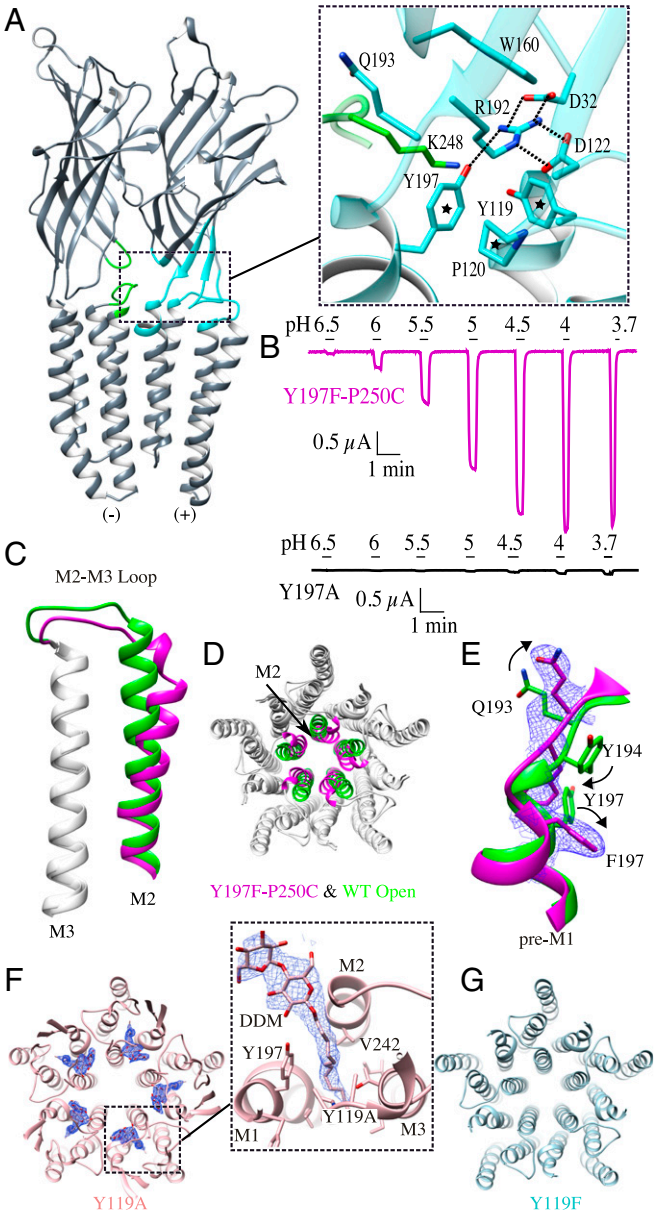

Fig. 5. The two electrostatic triads at the ECD–TMD interface governing channel gating. (*A*) Side view of two subunits of GLIC viewed from the outside of the pentamer. *Inset* shows a zoomed-in view of the interresidue electrostatic network at the ECD–TMD interface. The salt bridges formed between R192, D122, and D32 are shown in dashed lines. Hydrophobic stacking interactions between residue Y197, P120, Y119 (Cys-Loop) are also highlighted by a star. The interaction between the primary electrostatic triad and the secondary electrostatic triad through Y197 (pre-M1) and R192 is shown in dashed lines. (*B*) Proton-elicited currents of GLIC Y197F and Y197A. (*C*) Conformational change of Y197F mutant structure (purple) in the M2 helix and the M2-M3 loop compared with the GLIC wild-type (green). (*D*) Top view of the TMD. (*E*) Conformational rearrangement of the pre-M1 region. The electron density 2m*Fo*–D*Fc* map of the Y197F mutant structure (blue mesh) is contoured at the level of 1σ. (*F*) Top view of the structure of Y119A in the TMD region. The detergent molecules inserted into the intrasubunit cavity are shown as sticks with a blue mesh representation of the 2*Fo*–*Fc* electron density map in its vicinity contoured at 1σ and overlaid. The *Inset* zooms in on the zone of interaction of a detergent molecule with residues bordering the intrasubunit cavity. (*G*) Top view of the structure of Y119F in the TMD region.

molecule that we interpreted as a detergent molecule (DDM). DDM, which we used during the purification and crystallization of the receptor, is positioned in such a way that its sugar moiety is exposed to the ECD lumen and its hydrophobic tail inserts into the cavity vacated by the removal of the phenylalanine side chain (Fig. 5*F*, *Inset*). Therefore, we propose that in this case the hydrophobic tail of DDM fulfills the role of the aromatic ring of Y119 to artificially maintain the channel open. Interestingly, this cavity largely overlaps with the site that has been shown to contribute to the binding of propofol and desflurane (21).

We also explored the role of K248, which is involved in the secondary electrostatic triad, by solving the structures of K248C and K248A mutants. Their structures are wild-type-like at pH 4 (*SI Appendix*, Table S3): in K248C, the cysteine side chain is still able to make a hydrogen bond with Y197 and for K248A, N245 changes rotamer to make one more hydrogen bond with Y197, indicating a compensatory role of this site.

Mutations That Trap the Channel in the LC Form Reveal Two Different Networks That Stabilize the Open Form of the Channel Down to H235. ***One interfacial hydrophilic network connects E35 to the entrance of the channel pore (E243) and further down to H235.*** One of the results of the FD/DH calculations is the existence of a triad of strong electrostatic interactions involving Y119-Y197 and K248(+) (adjacent subunit) that extends the R192-D122-D32 well-known triad. Y197 can actually interact with two different M2-M3 loops, one from the same subunit (through L246) via the Cys-loop, and one from the adjacent subunit (through K248) (Fig. 5*A*, *Inset*). E243 marks the entrance of the channel. Strikingly, its side chain can adopt two different conformations in the open form (31). However, electrophysiology recordings show that E243C has almost the same pH_{50} value as the wild-type (18). Consistent with electrophysiology results, the E243C structure shows no distinguishable difference with the open form of GLIC (RSMD = 0.215 Å) (*SI Appendix*, Fig. S12*A*). To further probe the site of E243, the substitution E243G was generated: it results in a closed channel, similar to E243P, whose structure was previously reported to be in the LC2 conformation (*SI Appendix*, Fig. S12*C*). Collectively, our data suggest that E243 is probably not a key residue for proton sensing; rather, it is crucial for maintaining the stability of the upper part of the M2 helix during the channel opening. Strikingly, if one goes down the M2 helix starting at E243 by steps of four residues, on the same side of the helix, one finds N239 and H235, whose mutation in both cases stabilizes the LC form in the crystal (44). In conclusion, by connecting the dots between positions whose mutations trap the receptor in an LC form, the network Y197-K248-E243-N239-H235 further extends the network that originates from E35, Q193, and Y197, going deeply to the TMD of the adjacent subunit (Fig. 6*C*).

A different interfacial network that involves hydrophobic side chains connects E35 to the pre-M1 and to a TMD intrasubunit cavity known to bind general anesthetics. The hydrophobic network originating from the Y197-P120-Y119 interactions reaches out to L246 from the M2-M3 loop of the same subunit to build up a second ramification of the network connecting mutants stabilizing an agonist-bound but inactive form, in such a way that it completely encircles the ECD–TMD interface of the pentamer (Fig. 6*D*). Indeed, it contains residues close to L246 that have been mutated in previous studies and found to lead to the LC-form as well, namely P247G (17) and Y249 and T251 (16).

Upon channel opening, the tightly packed bundle of five M2 helices detach from each other and move closer to M3 helices. This reshapes a cavity located behind the M2 helix and beneath the residues Y197-P120-Y119, which is essential for general anesthetics binding (21). Structure analysis predicted that the mutation I201W (pre-M1), introducing a bulky amino acid in that cavity, would block the M2 helix movement. Indeed, the mutant I201W generates a nonfunctional receptor (18). The crystal structure of I201W shows an LC conformation, the same as that of E243G (*SI Appendix*, Figs. S12*B* and S13). In the open form of GLIC, the side chain of I201 contacts the hydrophobic residue F238 (F14′), L241 (L17′), and V242 (V18′) within the M2 helix of the same subunit (*SI Appendix*, Fig. S12*E*). The new bulky residue in I201W occupies this cavity and hinders the movement of the upper part of the M2 helix. Hence, this tightly packed hydrophobic network is also important for GLIC function and its modulation by pharmacological reagents.

Discussion

The structures of pairs of open and closed forms of the ion channel, in the case of GLIC (12, 14, 19), GluCl (4, 5), and GlyR (9) open the way to an understanding of the conformational transitions that take place during gating in pLGICs. Previous work has focused on normal mode analysis and coarse-grained methods to predict possible transition pathways from pairs of structures and simplified models of the proteins based on a mixture of elastic network models (19, 45). In addition, experimental studies, such as the measurement of the coupling ϕ-values using site-directed mutagenesis and patch clamp electrophysiology can provide detailed models of the sequence of events leading to the opening of the channel (46, 47). Furthermore, time-resolved fluorescence-quenching experiments can give information on the conformational transitions of the receptors in the millisecond scale (18). Fully atomistic molecular dynamics studies have also been used on the TMD alone (48) or on the full GluCl receptor, either for the gating or ungating transition (49, 50). Recently, molecular dynamics simulations were used to generate possible transition pathways for the gating in GLIC through the string method (51). For pH-gating, however, there is an additional difficulty in assigning the protonation state of all Asp, Glu, and His residues in the two end states. Presently, it is not known with certainty which of these residues are protonated concomitantly with the conformational transition, and current molecular dynamics experiments do not allow the (reversible) change of protonation state of titratable residues during simulations of such large systems. Therefore, more experimental studies are needed to help resolve this question.

Our studies do not contain any temporal information; however, they reveal a crucial proton-sensing residue, from which we progressively build up and extend a network of interactions that are essential for the stabilization of the open form. In that regard, we do not support the search for an "allosteric network" that would propagate information from the orthosteric site to the channel itself (52) and confine ourselves to the strict theory of allostery, which postulates a global transition between two forms of the same macromolecule (resting and active). Here, we could determine the K_D between the two forms in the absence of the ligand, which shows the presence of 5% of the bound form without any ligand. Strikingly, residues whose mutations perturb this equilibrium form a network of spatially connected residues. This network potentially provides a framework for the interpretation of a large body of experimental data.

The Proton-Sensing Residue Is Located Opposite Loop F and May Bypass the Classic Agonist-Binding Site. One of the major questions in the GLIC gating transition is to identify its proton sensors. It has been known for some time that several regions at the ECD–TMD interface are crucial for the gating transition (17). However, the exact role of all 34 carboxylate residues in the conformational change that occurs upon dropping the extracellular pH has remained elusive up to now. To identify the proton-sensing residues responsible for the gating transition, systematic site-directed mutagenesis of all Asp or Glu residues was undertaken, followed by both functional and structural characterization of the mutants (39). These studies have an inherent limitation in that only the global pH_{50} of the transition is measured, for all of the remaining Asp and Glu (53). Here we go further by using

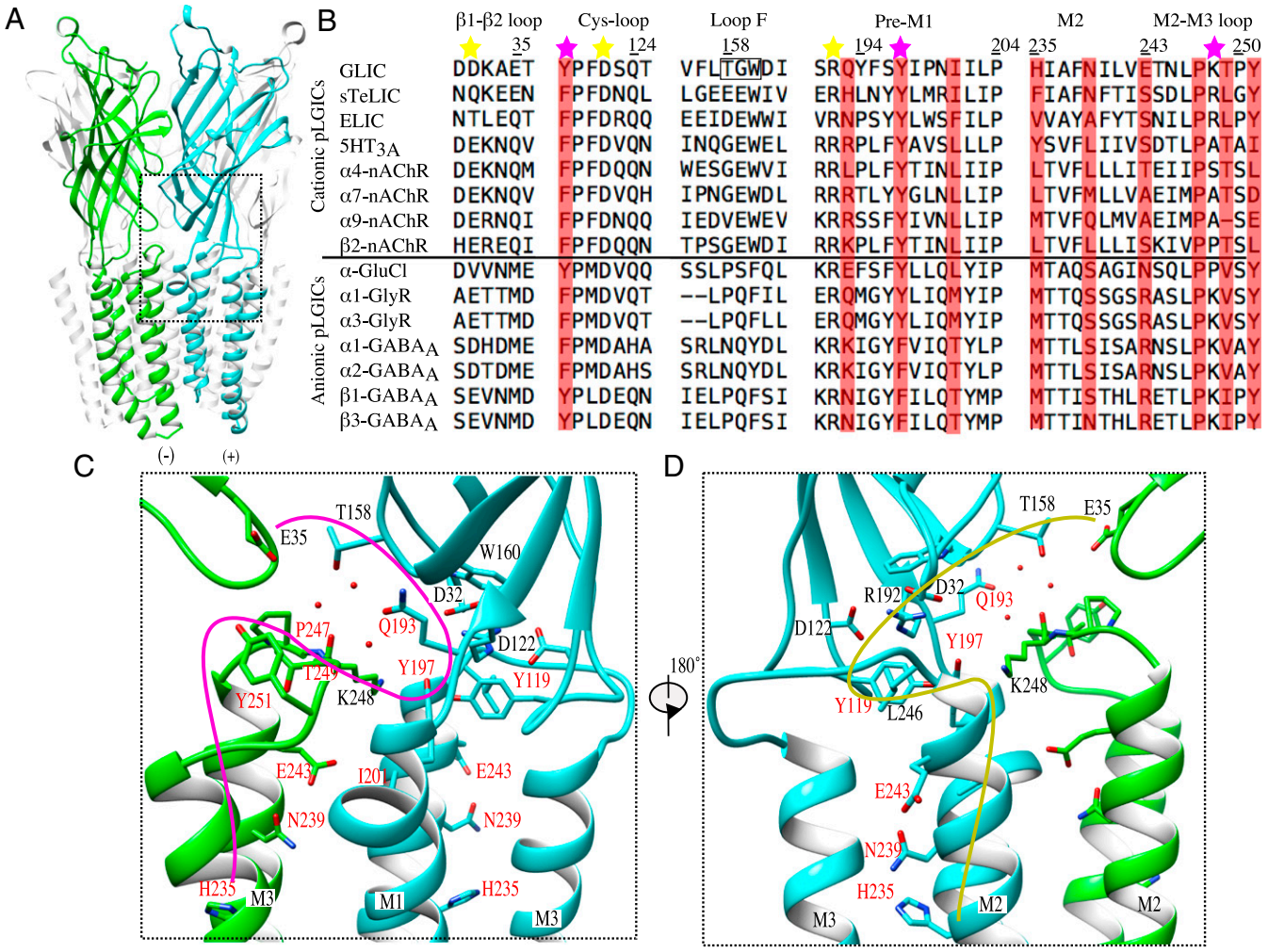

Fig. 6. Two stabilization networks are used in GLIC to maintain the channel open. (*A*) View of the GLIC wild-type open-form structure. Two adjacent subunits are highlighted. (*B*) Multiple-sequence alignment of GLIC and its homologs in a limited set of regions to highlight the positions in GLIC (colored in red) whose mutation traps GLIC in LC conformation. The alignment contains GLIC (*G. violaceus*) and ELIC (*E. chrysanthemi*), sTeLIC (symbiont of the worm *Tevnia*), GluCl (a glutamate-gated chloride ion channel from *Caenorhabditis elegans*), α1-GlyR (the glycine receptor α1 subunit from zebrafish), and $5HT_{3A}$ (the serotonin receptor from mouse). The remaining sequences are representatives for human pLGICs. Numbering refers to the GLIC protein sequence. The yellow stars indicate the residues forming the primary electrostatic triad and the purple stars indicate residues involved in the secondary electrostatic triad. The TGW motif in GLIC is boxed. (*C* and *D*) Two branches of a continuous network originating from E35 that reach, independently, the middle transmembrane region (H235) of two adjacent subunits. The proton-sensor E35 and key residues responsible for channel activation are shown as sticks. (*C*) View from outside the pentamer with the first network shown as a purple line, across subunits. (*D*) View from inside the pentamer showing the second network involving the hydrophobic cluster as an orange line, within the same subunit.

pH-induced FTIR spectroscopy and difference spectra to individually titrate a list of candidate Asp/Glu residues selected computationally by detailed electrostatic calculations.

E35 stands out as the main proton-sensor. It is located at the end of the β1-β2 loop and interacts with loop F of the next subunit through residue T158. Experiments involving the chemical labeling of T158C with MMTS showed the importance of this residue for channel opening. This is similar to experiments performed on the same position in ELIC, which also lead to the conclusion that this position is very important for the gating transition (26). Loop F has been shown to be responsible for the inhibition of some pLGICs by divalent ions, such as Ca^{2+} ions for ELIC and for nAChR, and Zn^{++} for GABA-R (52–56). Recently, Ulens and colleagues (57) showed that one should distinguish between the upper loop F binding site, occupied by bromoform in ELIC and xenon in GLIC, and the lower loop F binding site, occupied by chlorpromazine. Strikingly, examination of the GLIC structure strongly suggests that mutation to W160 in loop F will affect the stability of the R192-D122-D32 salt bridge due to the stacking interaction between the side chains of R192 and W160. Furthermore, compared with the resting state of GLIC, a marked backbone shift of loop F is observed in the open state of GLIC (19). In addition, electron paramagnetic resonance studies showed that big movements of loop F occur during activation in GLIC (29, 58).

In the eukaryotic pLGIC family, the gating equilibrium is governed by neurotransmitter binding to the loop C/loop B region (59). The key proton sensor E35 is not close to loop C and loop B. The backbone of loop C also shifts markedly between the open and closed states. We propose that proton-gating in GLIC bypasses the classic orthosteric site and that, instead, a consequence of the "bidirectional effect" in allostery [or "reciprocity principle" (60)] is observed, whereby the modification of loop F would be concomitant with (but not driven by) a rearrangement of loop C similar to what is observed in a pLGIC gated by a neurotransmitter.

Table 1. Structural mapping of the mutations that trap GLIC in a LC conformation

Variant	Location	Conformation (phenotype)	Note
Q193C+MMTS	Pre-M1	LC1 (loss-of-function)	Present study
Q193L	Pre-M1	LC1 (loss-of-function)	Present study
Q193M	Pre-M1	LC1 (loss-of-function)	Present study
Y197F-P250C	Pre-M1	LC1 (wild-type phenotype)	Present study
I201W- E243C	Pre-M1	LC2 (nonfunctional)	Present study
H235F (H11′F)	Upper M2	LC1 (nonfunctional)	PDB ID code 3TLT
H235Q (H11′Q)	Upper M2	LC (loss-of-function)	PDB ID code 5NJY
N239C (N15′C)	Upper M2	LC (loss-of-function)	PDB ID code 5NKJ
E243G (E19′G)	Upper M2	LC2 (nonfunctional)	Present study
E243P (E19′P)	Upper M2	LC2 (nonfunctional)	PDB ID code 3TLS
P247G (P23′G)	M2-M3 loop	LC2 (loss-of-function)	PDB ID code 5HEG
T249A (T25′A)	M2-M3 loop	LC1 (nonfunctional)	PDB ID code 4LMJ
Y251A (Y27′A)	M2-M3 loop	LC1 (nonfunctional)	PDB ID code 4MLM
Wild-type 10*His	C-terminal 10*His	LC and open coexist	PDB ID code 4NPP
K33C-T20′C	Loop2 and M2-M3 loop	LC1 (nonfunctional)	PDB ID code 3UU3
K33C-N21′C	Loop2 and M2-M3 loop	LC2 (nonfunctional)	PDB ID code 3TLW
K33C-L22′C	Loop2 and M2-M3 loop	LC3 (loss-of-function)	PDB ID code 3TLV
K33C-K24′C	Loop 2 and M2-M3 loop	LC1 (nonfunctional)	PDB ID code 3TLU

Mapping Residues Stabilizing the LC Form Informs on the Transition Pathway. The crystal structures of the open and LC states of GLIC are both captured at pH 4. Because it is fully protonated and has a closed pore, the LC-form represents an "agonist-bound closed form" of GLIC; it was found in three variant forms, termed LC1, LC2, and LC3 (15). In the LC2 conformation (E243G and I201W in this study), the deformation of the end turn of M2 helices stabilizes the closed pore but the M2-M3 loop conformation is unaltered. In the LC1 conformation (Q193M/L, Q193C+MMTS, and Y197F in this study), the mutation in the pre-M1 region presumably impairs the coupling of the ECD and TMD, the M2 helix end turn is destabilized, and the M2-M3 loop conformation is changed. In the LC3 conformation the M2 helix is further destabilized at its C terminus. LC2 has been suggested to represent a preactivation form, as inferred by detailed kinetics studies of the transition (18). Recently, more mutations further down on the same face of the M2 helix, at positions N239 and H235, were also shown to lead to the stabilization of the LC1 form (44). Here we go further by producing mutants in the pre-M1 region that also stabilize the LC1 form at positions 193 and 197 (Table 1), extending the network of positions where a mutation can change the equilibrium between the two forms and providing a link with the proton-sensing residue E35. The open and LC1 forms actually coexist in the same crystal at pH 4 (19). This indicates a low-energy barrier between these two conformations such that single-point mutations can modify it with a clear readout (*SI Appendix*, Fig. S14 *D* and *E*). This unique property enables us to map the residues that are important for the stabilization of the open form.

Structure-Based Activation Model with Two Alternative Stabilization Networks Originating from the Same ECD Subunit Interface and Plunging into the TMD. If we simply connect together those positions where mutants adopt any of the LC forms, we can propose a model for the coupling between proton binding and channel gating. First, the ECD undergoes a conformational change stabilized by an increase of the proton concentration, probably starting with the protonation of E35 ($pK_a = 5.8$), when the pH is lowered from 7 to 4. This would be associated with several changes in the ECD–TMD interface: (*i*) a change in loop F (T158, G159, W160), also affecting R192 through its hydrophobic stacking interactions with the side chain of W160; (*ii*) the local rearrangement of the β1-β2 loop (including D32), tightening the D122-R192-D32 triple salt bridge; and (*iii*) the pre-M1 region (Q193) through the described water-mediated hydrogen bond network at the ECD–TMD interface, again affecting R192 directly. The R192 primary triad is also linked in the open form of GLIC to a secondary electrostatic triad involving Y197 (pre-M1), Y119 (Cys-loop), and the M2-M3 loop (K248) of the adjacent subunit (*SI Appendix*, Fig. S14 *A–C*).

On one side of Y197, the rearrangement of the M2-M3 loop through L246 is accompanied by a counter-clockwise movement of the upper portion of M2 helices that generates a conductive channel pore; this movement also reshapes the TMD intrasubunit cavity probed by general anesthetics (21). Together with other data on the M2-M3 loop (15), this supports the idea that the coupling between the pre-M1 region, Cys-loop, and M2-M3 loop is mediated, at least partly, by a hydrophobic cluster within each subunit that stabilizes the open form of the channel (Fig. 6*D*). On the other side of Y197, another electrostatic network involves Y119, K248 of the next subunit, as well as E243. Strikingly, H235 and N239 have been shown to also be a binding site for several general anesthetics that, in some mutants of GLIC, can switch the receptor back and forth from the open to the closed forms, when they bind (44) (Fig. 6*C*). Altogether, the network of residues stabilizing the LC forms both percolate to the center of the TMD region and circulate between subunits. Residues involved in the stabilization networks described here were also shown to strongly affect the activation energy between the open and closed forms of eukaryotic pLGICs (43). Thus, we anticipate that the same activation model should be a general feature of pLGICs.

Our findings underline the importance of electrostatics in understanding the conformational transitions of pLGICs. First, the binding of the charged neurotransmitter (a cation in 5HT3 or ACh, or a zwitterion in GABA or Gly) changes the interface between ECDs, which is known to be highly deformable (61), immediately followed by solvent relaxation and adaptation of the surface charges at the lipid–water interface. In this respect, the presence of two separate electrostatic triads at the ECD–TMD interface is perhaps not so surprising. Second, the opening of the channel also leads to a major change of the electrostatic energy, if one considers transmembrane helices as simple macrodipoles. Finally, the permeation of ions drastically changes the electrostatic energy by setting to zero the local transmembrane potential, thus leading to another conformational transition of the receptor, this time to the desensitized form, probably accompanied by the relaxation of the lipid–TMD interactions. We expect

that molecular dynamics simulations explicitly taking into account the difference of ionic concentrations on each side of the membrane will give further insight into the conformational transitions of pLGICs.

Materials and Methods

GLIC was expressed and purified crystallized according to the protocol described in Bocquet et al. (12). The electrophysiology experiments were performed on GLIC expressed in *Xenopus laevis* oocytes. FTIR experiments were carried out by reconstitution of GLIC and its variants in POPE/POPG lipids. Full materials and methods are available in *SI Appendix*.

ACKNOWLEDGMENTS. We thank the staff at crystallization platform of Institut Pasteur; staff at European Synchrotron Radiation Facility and Synchrotron-Soleil for excellent beamline facilities; and Marie Prevost and Solène Lefebvre for assistance during the manuscript revisions. J.H. acknowledges financial support by the German Research Foundation through SFB 1078 projects A1 and B3. Z.F. was supported by Agence Nationale de la Recherche Grant "Pentagate" ANR-13-BSV-8. H.H. was sponsored by the Chinese Scholarship Council and Institut Pasteur.

1. Corringer P-J, et al. (2012) Structure and pharmacology of pentameric receptor channels: From bacteria to brain. *Structure* 20:941–956.
2. Lee WY, Free CR, Sine SM (2009) Binding to gating transduction in nicotinic receptors: Cys-loop energetically couples to pre-M1 and M2-M3 regions. *J Neurosci* 29:3189–3199.
3. Sauguet L, Shahsavar A, Delarue M (2015) Crystallographic studies of pharmacological sites in pentameric ligand-gated ion channels. *Biochim Biophys Acta* 1850:511–523.
4. Althoff T, Hibbs RE, Banerjee S, Gouaux E (2014) X-ray structures of GluCl in apo states reveal a gating mechanism of Cys-loop receptors. *Nature* 512:333–337.
5. Hibbs RE, Gouaux E (2011) Principles of activation and permeation in an anion-selective Cys-loop receptor. *Nature* 474:54–60.
6. Miller PS, Aricescu AR (2014) Crystal structure of a human GABAA receptor. *Nature* 512:270–275.
7. Huang X, Chen H, Michelsen K, Schneider S, Shaffer PL (2015) Crystal structure of human glycine receptor-α3 bound to antagonist strychnine. *Nature* 526:277–280.
8. Morales-Perez CL, Noviello CM, Hibbs RE (2016) X-ray structure of the human α4β2 nicotinic receptor. *Nature* 538:411–415.
9. Du J, Lü W, Wu S, Cheng Y, Gouaux E (2015) Glycine receptor mechanism elucidated by electron cryo-microscopy. *Nature* 526:224–229.
10. Hassaine G, et al. (2014) X-ray structure of the mouse serotonin 5-HT3 receptor. *Nature* 512:276–281.
11. Hilf RJC, Dutzler R (2008) X-ray structure of a prokaryotic pentameric ligand-gated ion channel. *Nature* 452:375–379.
12. Bocquet N, et al. (2009) X-ray structure of a pentameric ligand-gated ion channel in an apparently open conformation. *Nature* 457:111–114.
13. Jaiteh M, Taly A, Hénin J (2016) Evolution of pentameric ligand-gated ion channels: Pro-loop receptors. *PLoS One* 11:e0151934.
14. Hilf RJC, Dutzler R (2009) Structure of a potentially open state of a proton-activated pentameric ligand-gated ion channel. *Nature* 457:115–118.
15. Prevost MS, et al. (2012) A locally closed conformation of a bacterial pentameric proton-gated ion channel. *Nat Struct Mol Biol* 19:642–649.
16. Gonzalez-Gutierrez G, Cuello LG, Nair SK, Grosman C (2013) Gating of the proton-gated ion channel from *Gloeobacter violaceus* at pH 4 as revealed by X-ray crystallography. *Proc Natl Acad Sci USA* 110:18716–18721.
17. Bertozzi C, Zimmermann I, Engeler S, Hilf RJC, Dutzler R (2016) Signal transduction at the domain interface of prokaryotic pentameric ligand-gated ion channels. *PLoS Biol* 14:e1002393.
18. Menny A, et al. (2017) Identification of a pre-active conformation of a pentameric channel receptor. *eLife* 6:e23955.
19. Sauguet L, et al. (2014) Crystal structures of a pentameric ligand-gated ion channel provide a mechanism for activation. *Proc Natl Acad Sci USA* 111:966–971.
20. Basak S, Schmandt N, Gicheru Y, Chakrapani S (2017) Crystal structure and dynamics of a lipid-induced potential desensitized-state of a pentameric ligand-gated channel. *eLife* 6:e23886.
21. Nury H, et al. (2011) X-ray structures of general anaesthetics bound to a pentameric ligand-gated ion channel. *Nature* 469:428–431.
22. Sauguet L, et al. (2013) Structural basis for potentiation by alcohols and anaesthetics in a ligand-gated ion channel. *Nat Commun* 4:1697.
23. Laurent B, et al. (2016) Sites of anesthetic inhibitory action on a cationic ligand-gated ion channel. *Structure* 24:595–605.
24. Howard RJ, et al. (2011) Structural basis for alcohol modulation of a pentameric ligand-gated ion channel. *Proc Natl Acad Sci USA* 108:12149–12154.
25. Fourati Z, et al. (2017) Barbiturates bind in the GLIC ion channel pore and cause inhibition by stabilizing a closed state. *J Biol Chem* 292:1550–1558.
26. Nys M, et al. (2016) Allosteric binding site in a Cys-loop receptor ligand-binding domain unveiled in the crystal structure of ELIC in complex with chlorpromazine. *Proc Natl Acad Sci USA* 113:E6696–E6703.
27. Spurny R, et al. (2012) Pentameric ligand-gated ion channel ELIC is activated by GABA and modulated by benzodiazepines. *Proc Natl Acad Sci USA* 109:E3028–E3034.
28. Spurny R, et al. (2013) Multisite binding of a general anesthetic to the prokaryotic pentameric *Erwinia chrysanthemi* ligand-gated ion channel (ELIC). *J Biol Chem* 288:8355–8364.
29. Dellisanti CD, et al. (2013) Site-directed spin labeling reveals pentameric ligand-gated ion channel gating motions. *PLoS Biol* 11:e1001714.
30. Gielen M, Corringer P-J (2018) The dual-gate model for pentameric ligand-gated ion channels activation and desensitization. *J Physiol* 596:1873–1902.
31. Sauguet L, et al. (2013) Structural basis for ion permeation mechanism in pentameric ligand-gated ion channels. *EMBO J* 32:728–741.
32. Gielen M, Thomas P, Smart TG (2015) The desensitization gate of inhibitory Cys-loop receptors. *Nat Commun* 6:6829.
33. Mounsey KE, et al. (2007) Molecular characterisation of a pH-gated chloride channel from *Sarcoptes scabiei*. *Invert Neurosci* 7:149–156.
34. Beg AA, Ernstrom GG, Nix P, Davis MW, Jorgensen EM (2008) Protons act as a transmitter for muscle contraction in *C. elegans*. *Cell* 132:149–160.
35. Schnizler K, et al. (2005) A novel chloride channel in *Drosophila melanogaster* is inhibited by protons. *J Biol Chem* 280:16254–16262.
36. Thompson AN, Posson DJ, Parsa PV, Nimigean CM (2008) Molecular mechanism of pH sensing in KcsA potassium channels. *Proc Natl Acad Sci USA* 105:6900–6905.
37. Holzer P (2009) Acid-sensitive ion channels and receptors. *Handb Exp Pharmacol*, 283–332.
38. Sazanavets I, Warwicker J (2015) Computational tools for interpreting ion channel pH-dependence. *PLoS One* 10:e0125293.
39. Nemecz Á, et al. (2017) Full mutational mapping of titratable residues helps to identify proton-sensors involved in the control of channel gating in the *Gloeobacter violaceus* pentameric ligand-gated ion channel. *PLoS Biol* 15:e2004470.
40. Alqazzaz MA, Price KL, Lummis SCR (2016) Crotonic acid blocks the *Gloeobacter* ligand-gated ion channel (GLIC) via the extracellular domain. *Biochemistry* 55:5947–5951.
41. Prevost MS, et al. (2013) Identification of cinnamic acid derivatives as novel antagonists of the prokaryotic proton-gated ion channel GLIC. *J Med Chem* 56:4619–4630.
42. Hu H, et al. (2018) Crystal structures of a pentameric ion channel gated by alkaline pH show a widely open pore and identify a cavity for modulation. *Proc Natl Acad Sci USA* 115:E3959–E3968.
43. Lee WY, Sine SM (2005) Principal pathway coupling agonist binding to channel gating in nicotinic receptors. *Nature* 438:243–247.
44. Fourati Z, et al. (2018) Structural basis for a bimodal allosteric mechanism of general anesthetic modulation in pentameric ligand-gated ion channels. *Cell Reports* 23:993–1004.
45. Zheng W, Auerbach A (2011) Decrypting the sequence of structural events during the gating transition of pentameric ligand-gated ion channels based on an interpolated elastic network model. *PLOS Comput Biol* 7:e1001046.
46. Purohit P, Auerbach A (2007) Acetylcholine receptor gating: Movement in the α-subunit extracellular domain. *J Gen Physiol* 130:569–579.
47. Gupta S, Chakraborty S, Vij R, Auerbach A (2017) A mechanism for acetylcholine receptor gating based on structure, coupling, phi, and flip. *J Gen Physiol* 149:85–103.
48. Zhu F, Hummer G (2012) Drying transition in the hydrophobic gate of the GLIC channel blocks ion conduction. *Biophys J* 103:219–227.
49. Cecchini M, Changeux J-P (2015) The nicotinic acetylcholine receptor and its prokaryotic homologues: Structure, conformational transitions & allosteric modulation. *Neuropharmacology* 96:137–149.
50. Martin NE, Malik S, Calimet N, Changeux J-P, Cecchini M (2017) Un-gating and allosteric modulation of a pentameric ligand-gated ion channel captured by molecular dynamics. *PLOS Comput Biol* 13:e1005784.
51. Lev B, et al. (2017) String method solution of the gating pathways for a pentameric ligand-gated ion channel. *Proc Natl Acad Sci USA* 114:E4158–E4167.
52. Mowrey D, et al. (2013) Signal transduction pathways in the pentameric ligand-gated ion channels. *PLoS One* 8:e64326.
53. Di Russo NV, Estrin DA, Martí MA, Roitberg AE (2012) pH-dependent conformational changes in proteins and their effect on experimental pK(a)s: The case of Nitrophorin 4. *PLOS Comput Biol* 8:e1002761.
54. Zimmermann I, Marabelli A, Bertozzi C, Sivilotti LG, Dutzler R (2012) Inhibition of the prokaryotic pentameric ligand-gated ion channel ELIC by divalent cations. *PLoS Biol* 10:e1001429.
55. Galzi JL, Bertrand S, Corringer PJ, Changeux JP, Bertrand D (1996) Identification of calcium binding sites that regulate potentiation of a neuronal nicotinic acetylcholine receptor. *EMBO J* 15:5824–5832.
56. Hosie AM, Dunne EL, Harvey RJ, Smart TG (2003) Zinc-mediated inhibition of GABA(A) receptors: Discrete binding sites underlie subtype specificity. *Nat Neurosci* 6:362–369.
57. Delbart F, et al. (2018) An allosteric binding site of the α7 nicotinic acetylcholine receptor revealed in a humanized acetylcholine-binding protein. *J Biol Chem* 293:2534–2545.
58. Velisetty P, Chalamalasetti SV, Chakrapani S (2014) Structural basis for allosteric coupling at the membrane-protein interface in *Gloeobacter violaceus* ligand-gated ion channel (GLIC). *J Biol Chem* 289:3013–3025.
59. Plested AJR (2016) Structural mechanisms of activation and desensitization in neurotransmitter-gated ion channels. *Nat Struct Mol Biol* 23:494–502.
60. Schulze JO, et al. (2016) Bidirectional allosteric communication between the ATP-binding site and the regulatory PIF pocket in PDK1 protein kinase. *Cell Chem Biol* 23:1193–1205.
61. Nury H, et al. (2010) Crystal structure of the extracellular domain of a bacterial ligand-gated ion channel. *J Mol Biol* 395:1114–1127.